Supplementary Materials for

Morphodynamics of snow barchans at Concordia Station, Antarctica

Marine Poizat*, Jeanne Alkalla, Ghislain Picard, Laurent Arnaud, Daniel J. Nowacki, Simon Filhol, Eric Lefebvre, Clément Narteau

*Corresponding author: marine.poizat@gtk.fi
Paper DOI: 10.59236/geomorphica.v2i2.70

Table of Contents:

Supplementary Figures

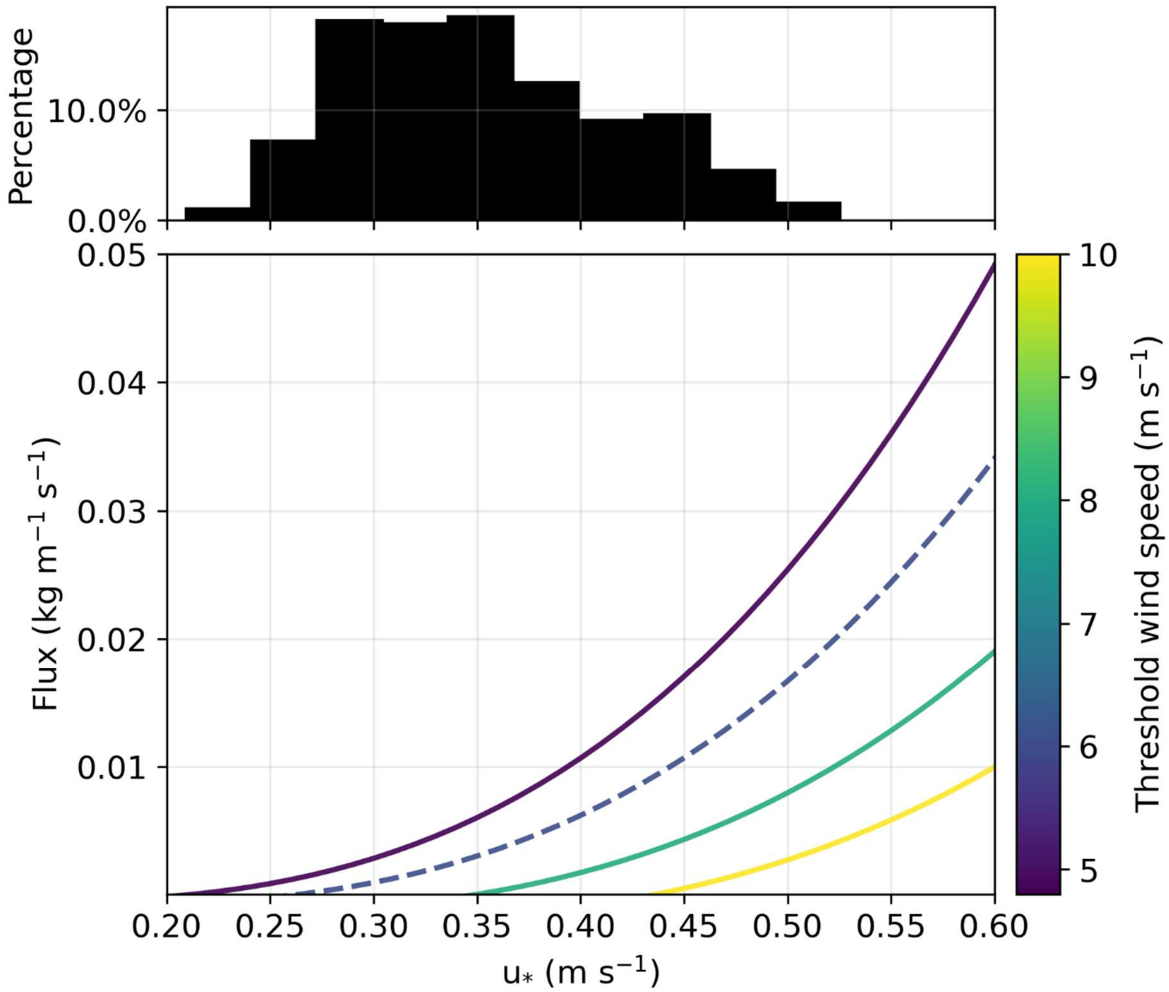

Figure S1.

(Bottom) Comparison of the flux from Schmidt (1982) for different threshold values. Dashed line is for a threshold speed of 6 m/s at 10 m height, which is the value used in the article. (Top) Distribution of the wind speed measured during barchan events, illustrating the range of conditions over which the transport models are evaluated.

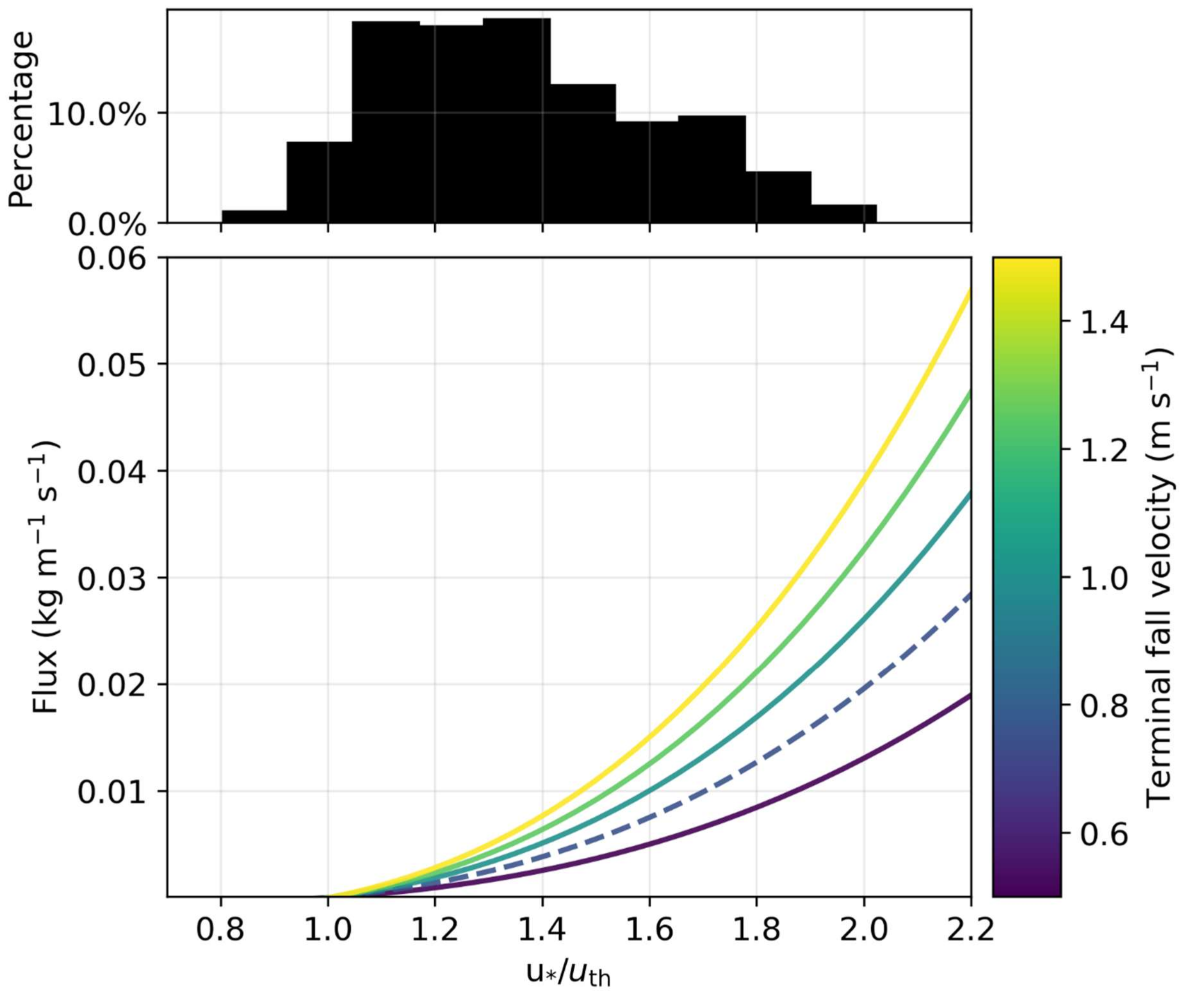

Figure S2

(Bottom) Comparison of the flux from Schmidt (1982) for different terminal fall velocity values as a function of friction velocity u_* normalized by the threshold friction velocity u_*^{th}. Dashed line is for a terminal fall velocity of 0.75 m/s, which is the value used in this study. (Top) Distribution of the wind speed measured during barchan events, illustrating the range of conditions over which the transport models are evaluated.

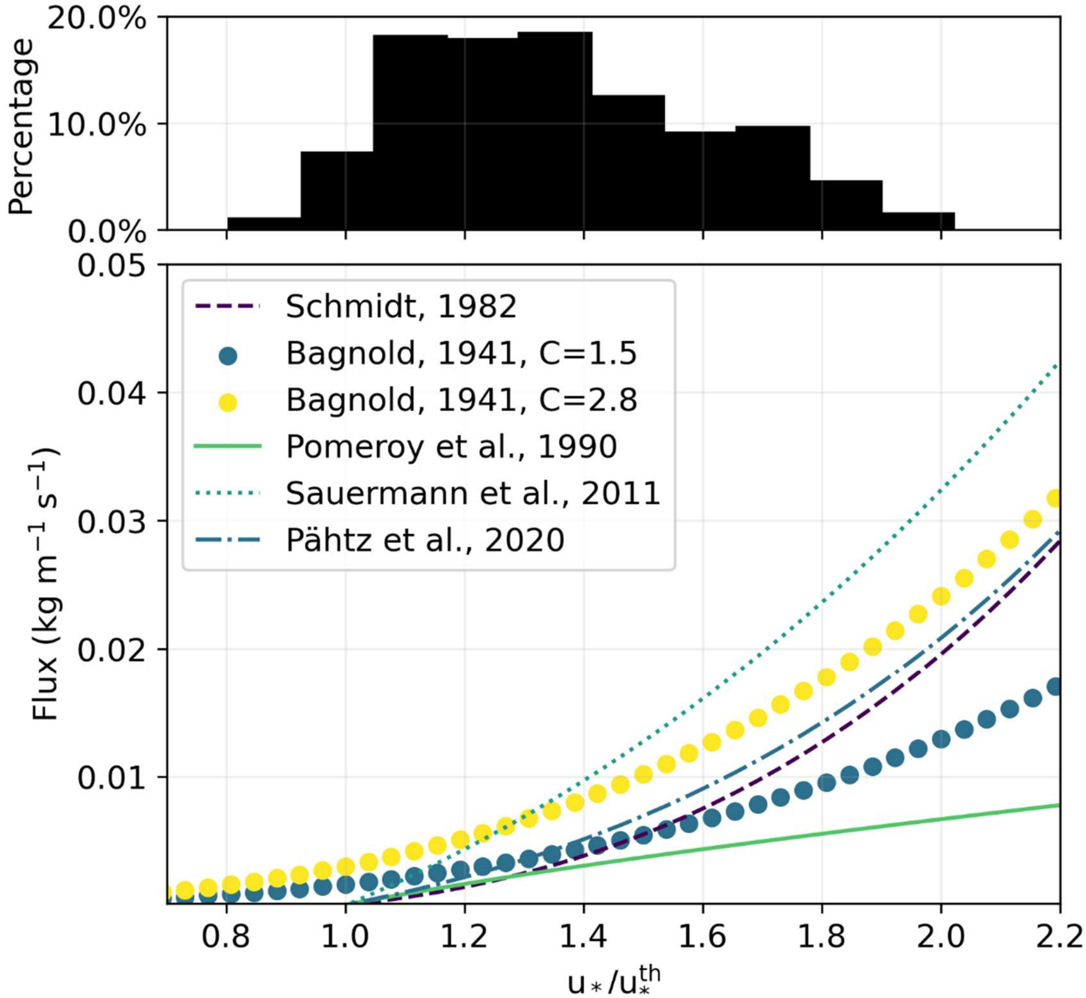

Figure S3

(Bottom) Comparison of the different flux relations as a function of friction velocity u_* normalized by the threshold friction velocity u_*^{th}. (Top) Distribution of the wind speed measured during barchan events, illustrating the range of conditions over which the transport models are evaluated.

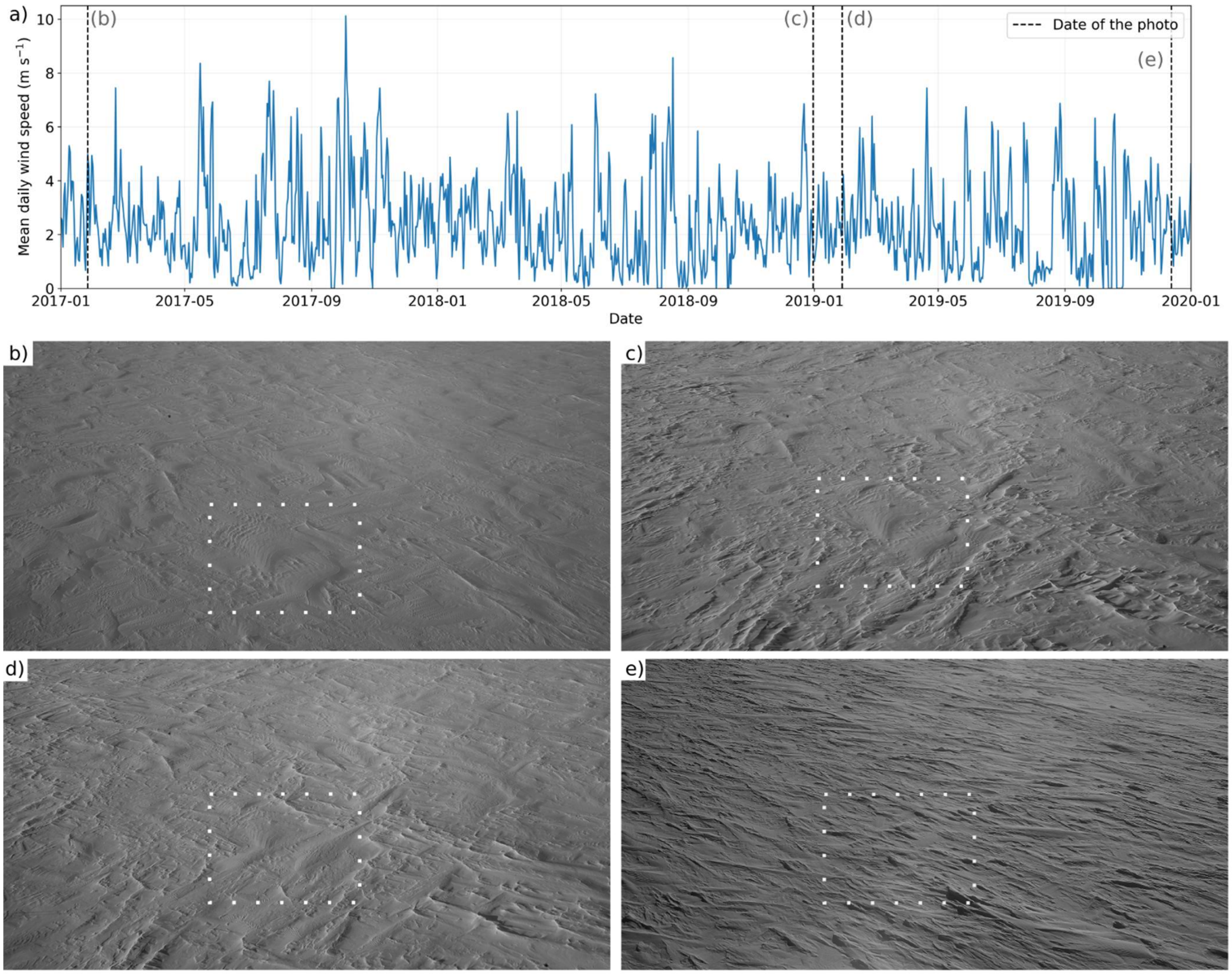

Figure S4

Three years of surface evolution at Concordia station. (a) Wind speed measured at the middle level (i.e., between 50 and 100 cm with respect to time. Raw images of the surface taken by near infra-red camera on (b) 28 January 2017, (c) 31 December 2018, (d) 28 January 2019, and (e) 13 December 2019. A sintered snow barchan, visible within the black dotted rectangle, progressively disappears over time. Between (b) and (c), a slight displacement of the observation area is visible, caused by routine maintenance of the tower or the near infra-red camera; this shift did not occur during the event analyzed.

Supplementary Tables

Table S1

List of some commonly used saltation mass flux relations.

Integrated mass flux (kg m^{-1}s^{-1})	Constant parameters	References	Friction velocity dependency
$Q_{PG} = C\frac{\rho_{\text{air}}}{g}u_*^{\text{th}}\left(u_*^2 - \left(u_*^{\text{th}}\right)^2\right)$	$C = 0.68$	Pomeroy and Gray et al., 1990	Quadratic
$Q_{Sc} = \frac{\rho_{\text{air}}}{g}\frac{u_{\text{f}}}{u_*^{\text{th}}}u_*^2(u_* - u_*^{\text{th}})$	$u_f = 0.75\ m/s$	Schmidt, 1982	Cubic
$Q_B = C\frac{\rho_{\text{air}}}{g}u_*^3\sqrt{\frac{d}{d_R}}$	$C = 1.5$ or $C = 2.8$	Bagnold, 1941	Cubic
$Q_{Sa} = 2\alpha\frac{\rho_{\text{air}}}{g}\left(u_*^2 - \left(u_*^{\text{th}}\right)^2\right)$ $(u_*\frac{2}{\kappa}\sqrt{\left(\frac{z_1}{z_m} + \left(1 - \frac{z_1}{z_m}\right)\frac{(u_*^{\text{th}})^2}{u_*^2}\right)} - \frac{2u_*^{\text{th}}}{\kappa} + u_{st})$	$C_d = 3$, $\alpha = 0.35$, $z_1 = 0.005$ m, $z_m = 0.04$ m	Sauermann et al., 2001	Cubic
$Q_P = \sqrt{\frac{2\Theta_{\text{th}}d\rho_{\text{air}}}{\kappa\mu(\rho_P - \rho_{air})g}}\left(u_*^2 - \left(u_*^{\text{th}}\right)^2\right)$ $\left(1 + \frac{\rho_{\text{air}}C_M}{gd\mu(\rho_P - \rho_{\text{air}})}\left(u_*^2 - \left(u_*^{\text{th}}\right)^2\right)\right)\rho_P$	Cm = 1.7	Pähtz et al., 2020	Quartic

References not cited in main manuscript

Pähtz, T. and Durán, O. Unification of aeolian and fluvial sediment transport rate from granular physics. Physical Review Letters, 124(16):168001, 2020

Pomeroy, J. W., & Gray, D. M. (1990). Saltation of snow. , 26 (7), 1583–1594. Retrieved 2021-11-10, from http://onlinelibrary.wiley.com/doi/abs/10.1029/WR026i007p01583 doi:10.1029/WR026i007p01583